J. Fluid Mech. (2009), *vol.* 620, *pp.* 167–175. © 2009 Cambridge University Press
doi:10.1017/S002211200800462X Printed in the United Kingdom

Boundary between unsteady and overturning ship bow wave regimes

GÉRARD DELHOMMEAU[1], MICHEL GUILBAUD[2], LAURENT DAVID[2], CHI YANG[3], AND FRANCIS NOBLESSE[4]†

[1]Laboratoire de Mécanique des Fluides, École Centrale de Nantes, CNRS, France
[2]Laboratoire d'Études Aérodynamiques, Université de Poitiers, ENSMA, CNRS, France
[3]Department of Computational and Data Sciences, George Mason University, Fairfax, VA, USA
[4]David Taylor Model Basin, NSWCCD, West Bethesda, MD, USA

(Received 17 July 2008 and in revised form 15 October 2008)

Measurements of the bow waves generated by a rectangular flat plate, immersed at a draught $D = 0.2$ m, towed at constant speed $U = 1.75$ m s^{-1} in calm water and held at a heel angle 10° and a series of nine yaw angles $\alpha = 10°$, 15°, 20°, 25°, 30°, 45°, 60°, 75° and 90° are reported. The measurements show that bow wave unsteadiness is significantly larger for the flat plate towed at yaw angles $30° \leqslant \alpha \leqslant 90°$ than at $10° \leqslant \alpha \leqslant 20°$, which are associated with the unsteady and overturning bow wave regimes, respectively, separated by the boundary $U/\sqrt{g\,D} = 4.4\,\tan\alpha\,/\cos\alpha - 1$ with $g \equiv$ acceleration of gravity. These measurements of bow wave unsteadiness provide preliminary experimental validation of the foregoing simple theoretical relation for the boundary between the unsteady and overturning bow wave regimes for non-bulbous wedge-shaped ship bows with insignificant rake and flare. Extension of this relation to more complicated ship bows, notably bows with rake and flare, is also considered.

1. Introduction

It is well know that a rigid body that advances at constant speed in a quiescent fluid does not necessarily generate a steady flow. The wake behind a body, notably a bluff body, is a classic example of this well-known property of fluid flows. An especially important and widely studied example of unsteady body wake is vortex shedding by a circular cylinder. Numerous other examples of instabilities and unsteadiness (associated with nonlinear effects) are found in fluid mechanics.

The specific example considered here is the bow wave generated by a ship that advances at constant speed U along a straight path in calm water. A ship bow wave is arguably the most visible, complex and important feature of free-surface flow about a ship and accordingly has been extensively studied: numerical and (to a lesser extent) experimental or analytical studies of ship bow waves are reported in Ogilvie (1973), Standing (1974), Chapman (1976), Miyata & Inui (1984), Çalişal & Chan (1989), Maniar, Newman & Xu (1991), Xu (1991), Tulin & Wu (1996), Dong, Katz & Huang (1997), Roth, Mascenik & Katz (1999), Fontaine, Faltinsen & Cointe (2000), Landrini, Colagrossi & Tulin (2001), Tulin & Landrini (2001), Waniewski, Brennen

† Email address for correspondence: francis.noblesse@navy.mil

https://doi.org/10.1017/S002211200800462X Published online by Cambridge University Press

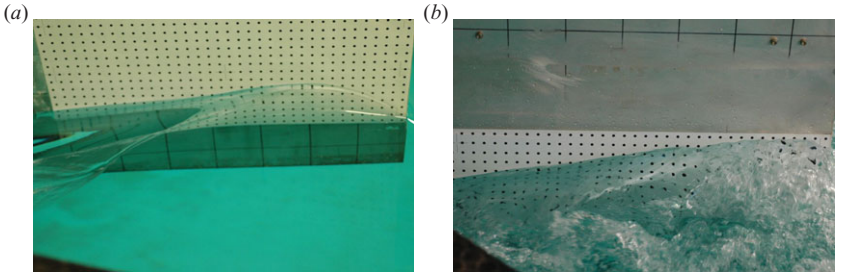


FIGURE 1. Examples of (*a*) steady overturning and (*b*) unsteady bow wave due to a vertical rectangular flat plate. The flat plate, immersed at a draught $D = 0.2$ m, is towed at a yaw (incidence) angle $\alpha = 15^\circ$ (*a*) or 45° (*b*) and a speed $U = 2.25$ m s^{-1} (*a*) or 2 m s^{-1} (*b*). The corresponding draught-based Froude numbers are $F \approx 1.61$ (*a*) and 1.43 (*b*). The values of α and F that correspond to these two photographs are marked with $\times$ in figure 2(*a*).

& Raichlen (2002), Karion *et al.* (2003), Muscari & Di Mascio (2004), Landrini (2006), Noblesse *et al.* (2006), Olivieri *et al.* (2007), Noblesse *et al.* (2008 *a, b*) and Shakeri *et al.* (2008).

However, whether a ship in steady motion generates a steady or unsteady bow wave is a basic issue that does not appear to have been examined in the literature, notably in the studies listed above, with the (recent) exception of Noblesse *et al.* (2008*b*). Yet, the issue is both of theoretical interest and of practical importance, notably for the decomposition of the drag of a ship into components associated with viscosity, wavemaking and wavebreaking and the appearance of a ship's wake and related ship signature.

Elementary fundamental theoretical considerations given in Noblesse *et al.* (2008*b*) lead to two main types of ship bow waves: 'overturning bow waves', which consist of thin sheets of water that are largely stable and steady (until the plunging waves hit the main body of water), and 'unsteady bow waves'. Examples of 'steady' overturning and unsteady bow waves – also widely called 'plunging' or 'spilling' waves in the literature – are shown on the left and right sides of figure 1. Other photographs of overturning and unsteady bow waves are shown in e.g. figure 6 of Noblesse *et al.* (2008*b*), where a simple theoretical relation for the boundary between the unsteady and overturning bow wave regimes is given for wedge-shaped ship bows (without bulb, rake or flare) with draught D and waterline entrance angle 2α.

This theoretical relation divides the flow domain $0 \leqslant \alpha$, $0 \leqslant F \equiv U/\sqrt{gD}$ into two regions separated by the boundary curve

$$F \equiv U/\sqrt{gD} = 4.4 \tan\alpha / \cos\alpha - 1, \tag{1.1}$$

where g stands for the acceleration of gravity. The curve defined by (1.1) is shown in figure 2. The bow wave generated by a wedge-shaped ship bow with a draught-based Froude number F and waterline entrance angle 2α that lies to the right of the curve (1.1) is necessarily unsteady, and this region is marked 'unsteady' in figure 2. The region between the boundary curve (1.1) and the axis $\alpha = 0$ corresponds to the overturning bow wave regime, where steady flow may exist. In other words, steady flow is not possible to the right of the curve (1.1), but unsteady flow is possible to the left of the curve. The curve (1.1) intersects the axis $F = 0$ for a waterline entrance angle $2\alpha \approx 25^\circ$. Thus, a ship with a fine bow, specifically with waterline entrance angle 2α smaller than approximately 25°, may generate a steady overturning bow wave at any speed. However, a ship with a fuller bow, with $25^\circ < 2\alpha$, can only generate a

https://doi.org/10.1017/S002211200800462X Published online by Cambridge University Press

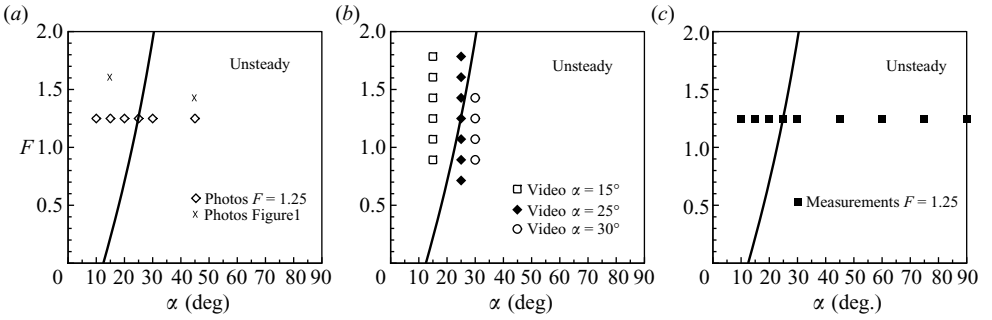


FIGURE 2. The curves in these three figures mark the theoretical boundary, defined by the relation (1.1), that divides the unsteady bow wave regime (on the right sides of the curves) and the overturning bow wave regime (between the curves and the vertical axis $\alpha = 0$). The symbols in the figures mark the draught-based Froude numbers F and the yaw angles α for which the bow waves due to a rectangular flat plate have been observed (photographs and videos) or measured (in this study). Specifically, the symbols $\times$ and $\diamond$ in (*a*) correspond to the two photographs shown in figure 1 and the six photographs shown in figure 6 of Noblesse *et al.* (2008*b*), respectively. The symbols in (*b*) correspond to videos for yaw angles $\alpha = 15°$, 25° and 30° at a series of Froude numbers: six Froude numbers $0.89 \leqslant F \leqslant 1.78$ for $\alpha = 15°$, seven Froude numbers $0.71 \leqslant F \leqslant 1.78$ for $\alpha = 25°$ and four Froude numbers $0.89 \leqslant F \leqslant 1.43$ for $\alpha = 30°$. (These three videos can be viewed at http://www.scs.gmu.edu/∼rlohner/pages/pics/freesurf.html.) Finally, the full squares in (*c*) correspond to the measurements of bow wave profiles, for $F = 1.25$ and nine yaw angles $\alpha = 10°$, 15°, 20°, 25°, 30°, 45°, 60°, 75° and 90°, which are considered here.

steady bow wave if the ship speed is higher than the critical speed defined (in terms of α) by the relation (1.1).

The division of ship bow waves into two complementary regimes – identified here as unsteady and overturning bow wave regimes – is not based on observed flow characteristics, i.e. on flow observations, but on theoretical considerations. Thus, the definition of these complementary regimes is 'theoretical' rather than 'experimental'. Specifically, the relation (1.1) that separates the two regimes is based on the upper bound $E\,g/U^2 \leqslant 1/2$ for the elevation E of the free surface for steady flows and a relation, given in Noblesse *et al.* (2006), for the height of the bow wave of a wedge-shaped ship bow. The boundary (1.1) is also shown in Noblesse *et al.* (2008*b*) to correspond to null flow velocity (in a frame of reference attached to the moving ship) at the crest of the bow wave.

Limited experimental validation of the theoretical relation (1.1) for the boundary between the unsteady and overturning bow wave regimes is given in figure 6 of Noblesse *et al.* (2008*b*), which shows six photographs of the bow waves due to a rectangular flat plate towed at a draught-based Froude number $F = 1.25$ (draught $D = 0.2$ m and speed $U = 1.75$ m s^{-1}), a heel angle 10° and a series of six yaw (incidence) angles $\alpha = 10°$, 15°, 20°, 25°, 30° and 45°. These six values of F and α are marked with $\diamond$ in figure 2(*a*). Videos of the bow waves due to the flat plate towed at yaw angles $\alpha = 15°$, 25° and 30° and a series of Froude numbers (six Froude numbers $0.89 \leqslant F \leqslant 1.78$ for $\alpha = 15°$, seven Froude numbers $0.71 \leqslant F \leqslant 1.78$ for $\alpha = 25°$ and four Froude numbers $0.89 \leqslant F \leqslant 1.43$ for $\alpha = 30°$) have also been made. The values of α and F that correspond to the three videos are marked in figure 2(*b*).

While these visual flow observations (photographs and videos) are interesting and useful – and consistent with the theoretical relation (1.1) for the boundary between the unsteady and overturning bow wave regimes – they are qualitative. Thus, an

https://doi.org/10.1017/S002211200800462X Published online by Cambridge University Press

experimental validation, based on measurements rather than visual observations, of (1.1) is needed. Although detailed experimental measurements of ship bow waves are reported in several of the previously listed experimental studies, notably Dong *et al.* (1997), Roth *et al.* (1999) and Shakeri *et al.* (2008), these experimental studies do not directly address the issue under consideration. Indeed, no systematic experimental investigation of the boundary between the unsteady and overturning ship bow wave regimes appears to have been reported in the literature. Simple measurements of bow wave unsteadiness, with the aim of seeking to test the validity of the theoretical relation (1.1) for the boundary between the unsteady and overturning ship bow wave regimes, are then reported here.

In this regard, it should be noted that the boundary (1.1) does not provide information about the degree of flow unsteadiness, although the analysis given in Noblesse *et al.* (2008*b*) indicates that a bow wave can be expected to be the more steady and stable, as $(\alpha\,, F)$ is located further to the left of the boundary curve (1.1). However, this theoretical boundary indicates that flow unsteadiness can be expected to be significantly greater for $(\alpha\,, F)$ located to the right (unsteady) side of the boundary curve, where a change of flow regime is predicted to occur, than to the left (steady overturning) side of the boundary. The purpose of the measurements reported here is precisely to test this prediction of a significant increase in flow unsteadiness, which can be taken as evidence of a flow regime change, as the boundary (1.1) is crossed.

2. Experimental measurements of bow wave unsteadiness

The experimental measurements of bow waves reported in Noblesse *et al.* (2006, 2008*a*, *b*) show that a rectangular flat plate immersed at a draught D and towed at an incidence (yaw) angle α with speed U generates a bow wave that closely resembles the bow wave due to a ship that advances at speed U and has a wedge-shaped bow with draught D and waterline entrance angle 2α. This analogy was used in the previously mentioned studies to expand the experimental database of bow wave measurements for wedge-shaped ship bows available in the literature. The analogy is again used here to investigate the bow wave unsteadiness and the related boundary (1.1) between the overturning and unsteady bow wave regimes.

Specifically, we consider the bow waves due to a rectangular flat plate, of length 0.782 m and height 0.5 m, immersed at a draught $D = 0.2$ m and held at a 10° heel angle (angle between the plate and the vertical axis). The flat plate is towed at a constant speed $U = 1.75$ m s^{-1} (draught-based Froude number $F \approx 1.25$), in the towing tank of the École Centrale de Nantes. Nine yaw angles $\alpha = 10°$, 15°, 20°, 25°, 30°, 45°, 60°, 75° and 90° are successively considered. The yaw angles $10° \leqslant \alpha \leqslant 20°$ and $30° \leqslant \alpha \leqslant 90°$ correspond to the overturning and unsteady bow wave regimes, respectively, to the left and right sides of the boundary curve in figure 2(*c*). The angle $\alpha = 25°$ lies on the boundary separating these two regimes.

For each of the nine yaw angles α, i.e. for each of the nine runs of the tow carriage, computer-driven colour photographs (8 for $10° \leqslant \alpha \leqslant 45°$, 10 for $\alpha = 75°$ and 90°, 11 for $\alpha = 60°$) of the bow wave were taken. The colour photographs were first transformed, using a greyscale, to sharpen the contrast between the plate and the bow wave. Next, corrections were made to account for projection effects and related geometric distortions due to the camera lenses. Circular markers (5 mm in diameter, spaced 2 cm apart horizontally and vertically) on the plate were used for this purpose. Specifically, a third-order camera model was determined, in a preliminary calibration, from the markers on a picture of the flat plate at rest and used in both the vertical

https://doi.org/10.1017/S002211200800462X Published online by Cambridge University Press

and the horizontal directions. This process resulted in a two-dimensional picture in a frame of reference attached to the plate. The errors associated with the process were estimated by measuring the distance between the projection of a marker on the plate and its actual position. These errors were used to quantify the quality of the camera model. The errors for the horizontal and vertical coordinates of the markers were found to be smaller than 0.5 mm and approximately 1 mm, respectively. The corresponding mean errors were approximately 0.002 mm and 0.02 mm, and the root mean square errors are approximately 0.1 mm and 0.32 mm, respectively, for the entire set of markers on the plate. Finally, the resulting black and white pictures were used to digitize (using digitization software) the contact curve between the plate and the bow wave, i.e. to determine the bow wave profile in a frame of reference attached to the plate. This operation was performed manually by clicking about 40 points along the curve on the computer screen. The coordinates of the points were automatically determined and saved in a data file.

Figure 3 shows the series of nine bow wave profiles determined as explained in the foregoing. There is little variation among the bow waves on the left side of figure 3, i.e. for the yaw angles $\alpha = 10^\circ$, 15° and 20° that correspond to the overturning bow wave regime according to the theoretical relation (1.1). Considerably more variation can be observed in figure 3 for $\alpha = 30^\circ$, 45°, 60°, 75° and 90°, which correspond to the unsteady bow wave regime defined by (1.1).

Two alternative quantitative measures of the variations among the bow waves shown in figure 3 are considered in figure 4. Specifically, figure 4(*a*) and 4(*b*) show the largest variation $Z_{max} - Z_{min}$ and the root mean square variation σ_z, respectively, among the bow waves shown in figure 3 for nine values $X = 50$, 100, 150, 200, 250, 300, 400, 500 and 600 mm of the distance from the leading edge of the plate. The range $0.16 \leqslant Xg/U^2 \leqslant 1.92$ corresponding to the range 50 mm $\leqslant X \leqslant$ 600 mm is marked by vertical lines in figure 3. Figure 4 shows that the largest variation $Z_{max} - Z_{min}$, and the root mean square variation σ_z are significantly larger for $30^\circ \leqslant \alpha \leqslant 90^\circ$ than for $10^\circ \leqslant \alpha \leqslant 20^\circ$.

This result is further illustrated in figure 5, where the values of $Z_{max} - Z_{min}$ and σ_z shown in figure 4 are averaged for $\alpha = 10^\circ$, 15° and 20° on one hand and $\alpha = 30^\circ$, 45°, 60°, 75° and 90° on the other hand. The resulting average values of $Z_{max} - Z_{min}$ and σ_z are marked 'overturning' and 'unsteady' in figure 5. The line marked 'boundary' in figure 5 corresponds to $\alpha = 25^\circ$. The ratios $\delta_z^{unsteady}/\delta_z^{overturning}$ and $\sigma_z^{unsteady}/\sigma_z^{overturning}$ of the 'unsteady' and 'overturning' average values of σ_z and $\delta_z \equiv Z_{max} - Z_{min}$ depicted in figure 5 are approximately equal to the values given in Table 1 for the nine values of X considered in figures 4 and 5. These ratios and figure 5 show that bow waves for $30^\circ \leqslant \alpha \leqslant 90^\circ$ exhibit a significantly higher degree of unsteadiness than bow waves for $10^\circ \leqslant \alpha \leqslant 20^\circ$, especially for small values of X near the leading edge of the plate.

3. Boundary between unsteady and overturning bow wave regimes for arbitrary ship hulls

The boundary (1.1) is based on the upper bound $Z_b\, g/U^2 \leqslant 1/2$ for steady free-surface flows and the relation

$$\frac{Z_b\, g}{U^2} \approx \frac{2.2}{1+F}\,\frac{\tan\alpha}{\cos\alpha} \tag{3.1}$$

for the height Z_b of the 'steady' bow wave (in the overturning bow wave regime). The relation (3.1) and the related boundary (1.1) can be used for a broad range of

https://doi.org/10.1017/S002211200800462X Published online by Cambridge University Press

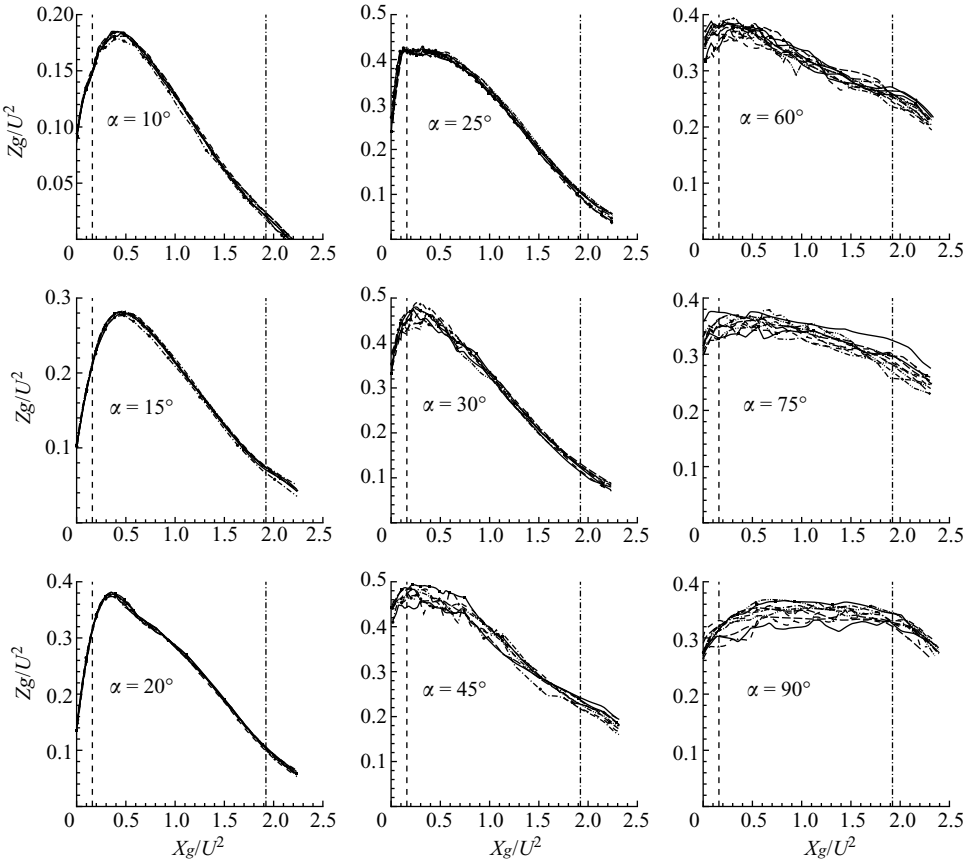


FIGURE 3. Bow waves due to a rectangular flat plate, immersed at a draught $D = 0.2$ m, towed at constant speed $U = 1.75$ m s^{-1} in calm water and held at a heel angle 10° and nine yaw angles $\alpha = 10°$, 15°, 20°, 25°, 30°, 45°, 60°, 75° and 90°. The waves for $\alpha = 10°$, 15° and 20° and for $\alpha = 30°$, 45°, 60°, 75° and 90° correspond to the overturning and unsteady bow wave regimes, respectively, to the left and right of the boundary curve shown in figure 2(*c*). The wave for $\alpha = 25°$ corresponds to the boundary between these two regimes.

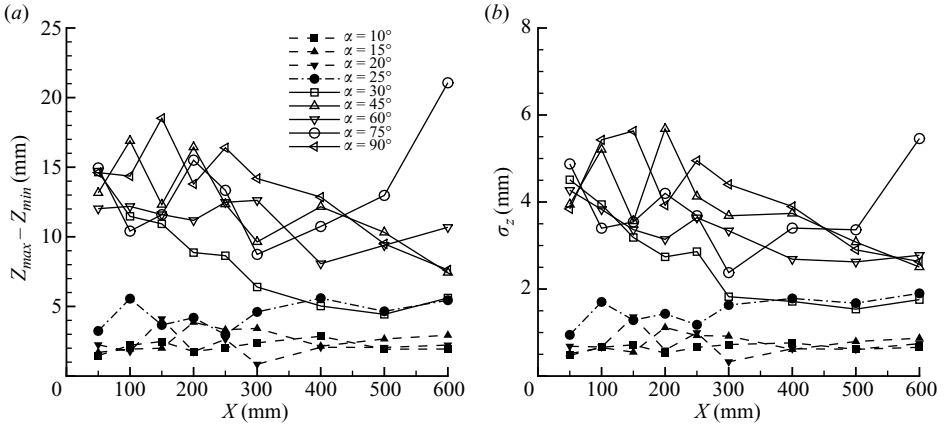


FIGURE 4. (*a*) Largest variation $Z_{max} - Z_{min}$ and (*b*) root mean square variation σ_z among the instantaneous bow wave profiles shown in figure 3.

https://doi.org/10.1017/S002211200800462X Published online by Cambridge University Press

X (mm)	50	100	150	200	250	300	400	500	600
$\delta_z^{unsteady}/\delta_z^{overturning}$	7.7	6.6	4.5	5.4	4.7	4.7	4.1	4.2	4.4
$\sigma_z^{unsteady}/\sigma_z^{overturning}$	7.7	6.6	4.4	5.3	4.5	4.8	4.6	4.0	4.0

TABLE 1. Ratios $\delta_z^{unsteady}/\delta_z^{overturning}$ and $\sigma_z^{unsteady}/\sigma_z^{overturning}$ of the 'unsteady' and 'overturning' average values of σ_z and $\delta_z \equiv Z_{max}-Z_{min}$ depicted in figure 5.

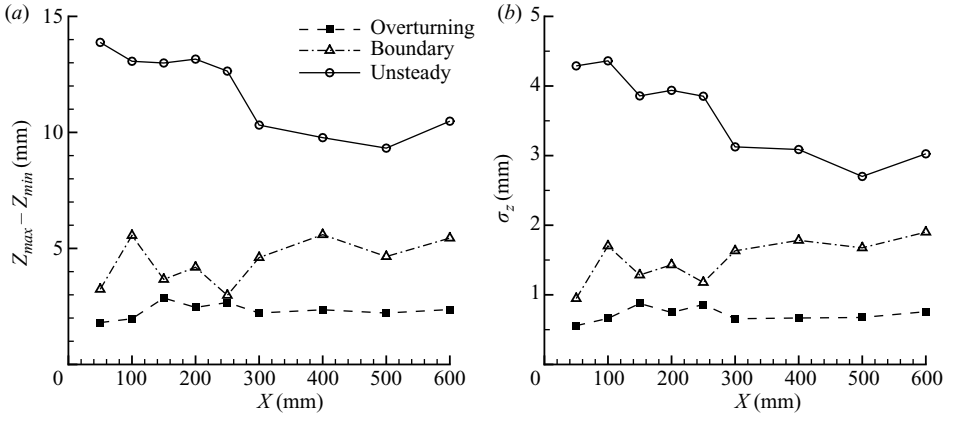


FIGURE 5. Averages of the variations (*a*) $Z_{max}-Z_{min}$ and (*b*) σ_z shown in figure 4 for $\alpha = 10°$, 15° and 20° and for $\alpha = 30°$, 45°, 60°, 75° and 90°. These averages correspond to the overturning and unsteady bow wave regimes, respectively, and are marked 'overturning' and 'unsteady' in the figure. The third curve in the figure, marked 'boundary', corresponds to $\alpha = 25°$, which lies on the boundary (1.1) between the overturning and unsteady wave regimes.

ship hulls, e.g. hull forms similar to the Series 60 ship model. However, these relations are not valid for ships with bulbous bows and for fast ships, which typically have bows with large rake and flare. They can be extended to more complicated ship bows (notably ship bows with appreciable rake and flare), using the upper bound $Z_b\, g/U^2 \leqslant 1/2$ and an estimate of the bow wave height Z_b, in the manner used in Noblesse *et al.* (2008*b*).

In particular, the influence of rake and flare on the bow wave height Z_b is considered in Noblesse *et al.* (in press) for a class of ruled ship bows, illustrated in figure 6, defined by four parameters: the draught D, the rake angle δ (the angle between the ship stem and the vertical axis) and the entrance angles 2α and $2\alpha'$ of the top and bottom waterlines (at the mean free surface $Z = 0$ and ship draught $z = -D$). For this four-parameter family of ship bows, which are reasonable approximations for a broad class of fast ships, the relation (3.1) can be extended as

$$\frac{Z_b\, g}{U^2} \approx \frac{2.2}{1+F}\,\frac{\tan\alpha+\tan\alpha'}{\cos\alpha+\cos\alpha'}\,\zeta_b(F,\delta,\varphi) \quad \text{with} \quad \varphi \equiv \frac{\tan\alpha-\tan\alpha'}{\tan\alpha+\tan\alpha'}\,. \tag{3.2}$$

The function $\zeta_b(F,\delta,\varphi)$ is determined in Noblesse *et al.* (in press) using thin-ship theory. There, ζ_b is given for six values of the draught-based Froude number F that correspond to $F/(1+F) = 0.3, 0.4, \ldots, 0.8$, nine rake angles $\delta = 60°, 45°, \ldots, -60°$ and nine values of the hull flare parameter $\varphi = 1, 0.75, \ldots, -1$. In the special case $\delta = 0$ and $\varphi = 0$ (i.e. $\alpha' = \alpha$), for which the four-parameter family of ship bows defined in figure 6 is identical to the two-parameter (draught D and waterline entrance angle

https://doi.org/10.1017/S002211200800462X Published online by Cambridge University Press

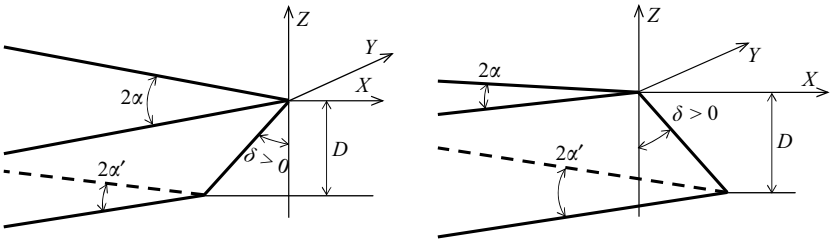


FIGURE 6. Four-parameter family of ship bows defined by the draught D, the top-waterline entrance angle 2α, the bottom-waterline entrance angle $2\alpha'$ and the rake angle δ.

2α) family of wedge-shaped bows (without rake and flare) considered in Noblesse *et al.* (2008*b*), we have $\zeta_b = 1$, and expressions (3.2) and (3.1) are identical as expected. The Bernoulli bound $Z_b\, g/U^2 \leqslant 1/2$ for steady free-surface flows and (3.2) then show that the boundary between the overturning and unsteady bow wave regimes is given by

$$F = 4.4\, \frac{\tan\alpha + \tan\alpha'}{\cos\alpha + \cos\alpha'}\, \zeta_b(F, \delta, \varphi) - 1\,. \tag{3.3}$$

This modification of (1.1) approximately accounts for the influence of rake and flare for ship bows that can be approximated by the four-parameter family defined in figure 6.

The boundary between the overturning and unsteady wave regimes for more general ship bows, notably bulbous bows, can be approximately determined in a similar manner, i.e. from the Bernoulli bound $Z_b\, g/U^2 \leqslant 1/2$ and an estimate of the bow wave height Z_b in the overturning bow wave regime. This estimate can be obtained using alternative steady-flow calculation methods, including semi-analytical theories based on various approximations (thin-ship, slender-ship, 2d+t theories), potential-flow panel (boundary integral equation) methods that rely on the use of a Green function (elementary Rankine source or Havelock source that satisfies the radiation condition and the Michell linearized free-surface boundary condition) and computational fluid dynamics (CFD) methods.

4. Conclusion

The measured experimental bow wave profiles for a rectangular flat plate towed at nine yaw angles $10^\circ \leqslant \alpha \leqslant 90^\circ$ exhibit a significantly higher degree of unsteadiness for $30^\circ \leqslant \alpha \leqslant 90^\circ$ than for $10^\circ \leqslant \alpha \leqslant 20^\circ$. These experimental measurements agree with the authors' previous visual flow observations (photographs and videos) and also with the theoretical relation (1.1) that defines the boundary between the unsteady and 'steady' overturning ship bow wave regimes.

Thus, the experimental measurements of bow wave unsteadiness reported here provide preliminary experimental validation of the theoretical relation (1.1) for the boundary between the unsteady and overturning ship bow wave regimes, also widely identified as plunging and spilling waves in the literature, for (non-bulbous) wedge-shaped ship bows (with insignificant rake and flare). Additional, more detailed, experimental validation would of course be useful, both for the simplest class of wedge-shaped ship bows considered here and for more complicated ship bows, notably wedge-shaped ship bows with rake and flare for which the boundary (1.1) can be modified as (3.3).

https://doi.org/10.1017/S002211200800462X Published online by Cambridge University Press

This work was partially funded by the Office of Naval Research (technical monitor Ms Kelly Cooper) and NSWCCD's ILIR program (technical monitor Dr John Barkyoumb).

REFERENCES

Çalışal, S. M. & Chan, J. L. K. 1989 A numerical modeling of ship bow waves. *J. Ship Res.* **33**, 21–28.

Chapman, R. B. 1976 Free surface effects for yawed surface-piercing plate. *J. Ship Res.* **20**, 125–136.

Dong, R. R., Katz, J. & Huang, T. T. 1997 On the structure of bow waves on a ship model. *J. Fluid Mech.* **346**, 77–115.

Fontaine, E., Faltinsen, O. M. & Cointe, R. 2000 New insight into the generation of ship bow waves. *J. Fluid Mech.* **321**, 15–38.

Karion, A., Sur, T. W., Fu, T. C., Furey, D. A., Rice, J. R. & Walker, D. C. 2003 Experimental study of the bow wave of a large towed wedge. In *Eigth Intl Conf. on Numerical Ship Hydrodynamics*, Busan, Korea.

Landrini, M. 2006 Strongly nonlinear phenomena in ship hydrodynamics. *J. Ship Res.* **50**, 99–119.

Landrini, M., Colagrossi, A. & Tulin, M. P. 2001 Breaking bow and stern waves: numerical simulations. In *Sixteenth Intl. Workshop on Water Waves and Floating Bodies*, Hiroshima, Japan.

Maniar, H., Newman, J. N. & Xu, H. 1991 Free-surface effects on a yawed surface-piercing plate. In *Eighteenth Symp. on Naval Hydrodynamics. Ann. Arbor*, MI. pp. 273–282.

Miyata, H. & Inui, T. 1984 Nonlinear ship waves. *Adv. Appl. Mech.* **24**, 215–288.

Muscari, R. & Di, Mascio, A. 2004 Numerical modelling of breaking waves generated by a ship's hull. *J. Marine Sci. Techol.*, **9**, 158–170.

Noblesse, F., Hendrix, D., Faul, L. & Slutsky, J. 2006 Simple analytical expressions for the height, location, and steepness of a ship bow wave. *J. Ship Res.* **50**, 360–370.

Noblesse, F., Delhommeau, G., Guilbaud, M., Hendrix, D. & Yang, C. 2008*a* The rise of water at a ship stem. *J. Ship Res.* **52**, 89–101.

Noblesse, F., Delhommeau, G., Guilbaud, M., Hendrix, D. & Yang, C. 2008*b* Simple analytical relations for ship bow waves. *J. Fluid Mech.* **600**, 105–132.

Noblesse, F., Delhommeau, G., Kim, H. Y. & Yang, C. In press. Thin-ship theory and influence of rake and flare. *J. Engng. Math.*

Ogilvie, T. F. 1973 The wave generated by a fine ship bow. *Ninth Intl Symp. on Naval Hydrodynamics.*

Olivieri, A., Pistani, F., Wilson, R., Campana, E. & Stern, F. 2007 Scars and vortices induced by ship bow and shoulder wave breaking *J. Fluids Engng.* **129**, 1445–1459.

Roth, G. I., Mascenik, D. T. & Katz, J. 1999 Measurements of the flow structure and turbulence within a ship bow wave. *Phys. of Fluids*, **11**, 3512–3523.

Shakeri, M., Maxeiner, E., Tavakolinejad, M. & Duncan, J. H. 2008 Characteristics of breaking bow waves generated by a 2D+T wave maker. In *27th Intl Symp. on Naval Hydrodynamics* Seoul, Korea.

Standing, R. G. 1974 Phase and amplitude discrepancies in the surface wave due to a wedge-ended hull form. *J. Fluid Mech.* **62**, 625–642.

Tulin, M. P. & Wu, M. 1996 Divergent bow waves. In *Twenty First Symp. on Naval Hydrodynamics*, Trondheim, Norway.

Tulin, M. P. & Landrini, M. 2001 Breaking waves in the ocean and around ships. In *Twenty Third Symp. on Naval Hydrodynamics.* Val de Reuil, France, pp. 1–32.

Waniewski, T. A., Brennen, C. E. & Raichlen, F. 2002 Bow wave dynamics. *J. Ship Res.* **46**, 1–15.

Xu, H. 1991 A potential flow solution for a yawed surface-piercing plate. *J. Fluid Mech.* **226**, 291–317.

https://doi.org/10.1017/S002211200800462X Published online by Cambridge University Press